

Erasure-tolerance scheme for the surface codes on Rydberg atomic quantum computers

Fumiyoshi Kobayashi^{1,2,*} and Shota Nahgayama^{3,4}

¹*Graduate School of Engineering Science, Osaka University,
1-3 Machikaneyama, Toyonaka, Osaka 560-8531, Japan.*

²*Center for Quantum Information and Quantum Biology,
Institute for Open and Transdisciplinary Research Initiatives, Osaka University, Japan.*

³*Mercari R4D, Mercari Inc., Roppongi Hills Mori Tower 18F,
6-10-1, Roppongi, Minato-ku, Tokyo 106-6118, Japan.*

⁴*Graduate School of Media and Governance, Keio University,
5322 Endo, Fujisawa-shi, Kanagawa 252-0882 Japan.*

(Dated: May 7, 2024)

Rydberg atom array with optical tweezers is a promising candidate for a fault-tolerant quantum computer, thanks to its good properties such as scalability, long coherence time and optical accessibility for communication. A big barrier to overcome is non-Pauli errors, erasure errors and leakage errors. Conventional work has revealed that leakage error is convertible to erasure error. A remaining problem is that such (converted) erasure errors continuously happen and accumulate. The previous proposal involved transporting atoms directly from the reservoir area, where atoms are stored for spare, to the computational area, where the computation and the error correction are processed, to correct atom loss. However, transporting atoms takes a long time and has side effects on surrounding qubits in practice. In this study, we evaluate the effects on planar code by circuit-based Monte Carlo simulation which has depolarizing errors and erasure errors, and propose a new scheme to tolerate that problem, namely, *k-shift erasure recovery* scheme. Our scheme uses online code deformation to tolerate erasures and repeatedly transfers the logical qubit from an imperfect array in which erasure errors accumulated to another perfect array in which erasure errors have been fixed by offline optical tweezers, to tolerate a large (accumulated) number of erasures. Furthermore, our scheme corrects erasure errors of atom arrays while logical qubits are evacuated from that area to correct; therefore, manipulating optical tweezers for erasure correction does not disturb qubits that compose logical data. We believe that our scheme provides practical directions for Rydberg atom quantum computers to realize feasible fault-tolerance.

I. INTRODUCTION

Scalable and universal quantum computers are expected to be the computers for the next generation beyond classical computers. Rydberg atomic quantum computers are particularly promising candidates for scalable quantum computers, as they demonstrated key functionalities required for fault-tolerant quantum computation [1, 2]. Rydberg atoms have desirable properties as qubits, such as long coherence time and high controllability in the array. However, there are typical hurdles to overcome, erasing of atoms, which is the disappearance of qubits caused naturally by the escape of atoms on which the qubit is encoded from optical tweezers, and leakage errors, which are the leakage of atom states from computational quantum state space caused by such as imperfect operation of Rydberg interactions applied to execute quantum gates.

In addition, it has been shown that leakage errors and atom loss are detectable by Rydberg gates [3], and a method to convert leakage errors to erasure errors by Rydberg excitation has also been proposed [4–6]. Thus, the atom loss and leakage errors can be treated as erasure

errors by the above techniques.

Fortunately, surface codes are known to have a tolerance to erasure errors using super stabilizers [7, 8]. However, those studies have not revealed the limitation of surface code when erasure errors increase dynamically and accumulate on an array. This behavior is commonly observed in Rydberg atom quantum computers. Another problem in acquiring the erasure tolerance for surface code is how to refill vacant spots with atoms. In previous studies, atoms were refilled directly into the online array on which some error correction code is encoded [3, 4]. However, this procedure may have problematic side effects on dense arrays; it may cause erasure errors when the transposed atoms are close to other atoms on the array ($a < 5 \mu\text{m}$) [9]. It means that refilling atoms directly into the online array causes additional errors if an error-correcting code such as surface code is implemented on a dense array. Repairing erased atoms may result in a high possibility of transversal Pauli error chains which is a typical source of the logical error of the surface code, leading to a high logical error rate.

In this study, we evaluate the performance of planar code which has depolarizing errors and dynamically accumulating erasure errors by circuit-based Monte Carlo simulation. This simulation assumes dense arrays and ancillary qubits can be non-destructively measured. The simulation shows that the surface code on the array, on

* fkobayashi@qi.mp.es.osaka-u.ac.jp

which vacant spots are refilled only when offline, does not have the threshold of logical error rate and has just a pseudo-threshold of physical error rate for logical error rate. Our surface code has the pseudo-threshold, not the threshold, because the number of operations increases and the accumulated erasure errors increase on the array. The surface code repeats error syndrome measurements and decoding as many times as the code distance to correct Pauli errors on ancilla qubits and measurement errors. As a result, the number of accumulated erasure errors on the array increases along with the time executing the error detecting and correcting operations of surface code.

To solve this problem, we propose a new scheme to tolerate erasures, namely *k-shift erasure recovery*. Our scheme protects the logical state from erasure errors by combining the code deformation technique of the surface code, which are extension and contraction operations, and the atom transportation to rearrange or refill atoms on the array. This scheme maintains the array without caring about the decoherence of qubits caused by the atom transportation of tweezers, thanks to separating the operation to maintain the logical qubit from the maintenance of the atom array. This transportation of a logical qubit is realizable by not only lattice surgery but also quantum teleportation including methods using transversal CNOT gates.

Recently, yet another approach to addressing erasure qubits has been demonstrated, wherein atoms are coherently transported without disturbing surrounding qubits in a sparse array on which Rydberg interactions do not reach unless moving atoms [1, 2]. On the other hand, our approach considers the erased qubits on dense arrays where Rydberg interactions work between beyond nearest-neighbors and non-destructive measurements.

Our scheme helps to develop Rydberg quantum computers into fault-tolerant quantum computers by protecting a logical quantum state from both Pauli error and erasure error.

II. RYDBERG ATOM QUBITS 2-D ARRAY AND ITS ERROR MODEL

The atomic species used in the neutral atom quantum computer are alkali metals such as Rb and Cs, and alkaline earth metals such as Yb and Sr. These atoms are called Rydberg atoms because their interactions are controllable by being excited to Rydberg states which are states of a large principal quantum number. Using this interaction, multi-qubits gates can be implemented by Rydberg blockade [10, 11].

An optical tweezer is a technique to trap a single atom on a spot focused μm width, which is shaped by a spatial light modulator (SLM), an acousto-optic deflector (AOD), and an objective lens [11]. The tweezer array can arrange many single atoms at once and can control the shape of the array and the distance between atoms

freely [12]. In addition, it is possible to transport a single atom by moving the optical tweezer potential by manipulating SLM and AOD [1].

A. Rydberg atom qubits

A single atom has multiple energy levels, and two of them are determined to define a qubit, such as the levels on a hyperfine structure. An arbitrary single-qubit gates are realized using Rabi oscillation on qubit sublevels [11]. Multi-qubit gates are realized via a dipole-dipole interaction between Rydberg states, and they are called the Rydberg gates. Let r be the distance between atoms. The dipole-dipole interaction decreases depending on $1/r^6$. The Rydberg gates are applicable among atoms which are not necessary to be nearest-neighbors in the array as long as they are close enough for the dipole interaction to act effectively. The typical two-qubit gate of Rydberg gate is CZ gate [10]. A CNOT gate is achievable by a CZ gate headed by and followed by Hadamard gates to the target qubit. Combining those arbitrary single-qubit gates and multi-qubit gates, a universal quantum gate set is achieved on Rydberg atom quantum computers.

B. Leakage errors and atom loss on neutral atom qubits, and erasure errors

Atomic quantum computers with optical tweezer arrays are not only exposed to Pauli errors on the qubit space but also leakage errors where the state leaks to outside levels of the qubit space, and atom loss where atoms are erased, such as disappearing from optical tweezer sites. Some leakage states can be corrected to the qubit space by optical pumping [3], and other leakage errors can be converted to erasure errors if their occurrence is detected [4]. A 2-electron neutral atom has demonstrated the erasure conversion protocol for leaked states of radiative decay and blackbody radiation error [5, 6].

The atom loss is the atom's disappearance from the tweezer site. The existence of an atom on the site is detectable by quantum circuits such as shown in Fig. 1 with an ancilla qubit [3]. Thus, atom loss can also be treated as erasure errors.

Combining those discussions, physical errors which include both leakage errors and atom loss are treated as erasure errors in the software domain of error correction as long as their occurrence is detectable. By erasure error, quantum states ρ are mapped to non-qubit space by probability p_e , i.e.

$$\mathcal{E}_e(\rho) = (1 - p_e)\rho + p_e |e\rangle \langle e|, \quad (1)$$

where $|e\rangle$ is a state on non-qubit space [13].

In the case of the CZ gate operation with a completely erased qubit, the CZ gate does not work at all, so it is equivalent to the Identity gate, so it does not cause state error.

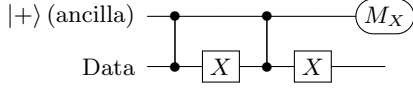


FIG. 1. The circuit to detect an erased data qubit by Rydberg gates with an additional ancilla qubit [3].

III. SURFACE CODE WITH ERASURE ERRORS

A. Surface code

The surface code is one of the topological quantum error correction codes [14, 15]. Let us consider a qubit array arranged on a square lattice in which the data qubits (white circle) are on each edge and the ancilla qubits for the error syndrome measurements (blue and orange circle) are on face and vertex as shown in Fig. 2a. To define the stabilizer group of the surface code for an ideal array without erasures $\mathcal{S}_{\text{ideal}}$, we define the star and plaquette operators

$$X_s = \bigotimes_{e \in \partial^* v} X_e, \quad Z_p = \bigotimes_{e \in \partial p} Z_e, \quad (2)$$

where v, e, p are the vertices, edges, and faces of the square lattice, and ∂, ∂^* are the boundary operators of the square lattice and its dual lattice, respectively. The boundary of the code is classified into two types, called the smooth boundary where X_s ends up, and the rough boundary where Z_p ends up.

B. Error detection and decoding

The encoded state $|\psi_L\rangle$ is stabilized by \mathcal{S} as constructed above. The errors on this state are determined by the measuring eigen-values corresponding to the stabilizer generators $S \in \mathcal{G}$ whether +1 or -1, which provides information about the Pauli errors that occurred in the qubit array. By performing indirect measurements of the star (plaquette) operator as in Fig. 2c via the orange (blue) auxiliary qubits in Fig. 2a, we obtain this information. This measurement is called syndrome measurement. A set of one trial of syndrome measurement corresponding to each element of \mathcal{G} constructed as above is called *Big-T*. For a planar code with code distance d , perform d sets of Big-T syndrome measurements.

Even if measurement errors occur during syndrome measurements, repeating syndrome measurements d times makes the logical qubit tolerant against measurement errors.

The error syndromes contain the information of errors. To decode those syndromes into Pauli errors, we form the graph \mathcal{N} as shown in [16] and it is called \mathcal{N} a *Nest*. At first, regard each syndrome as a vertex in \mathcal{N} . Then, Connect these vertices to the edge that corresponds to a spacial, Pauli error on each data qubit. Also, connect the

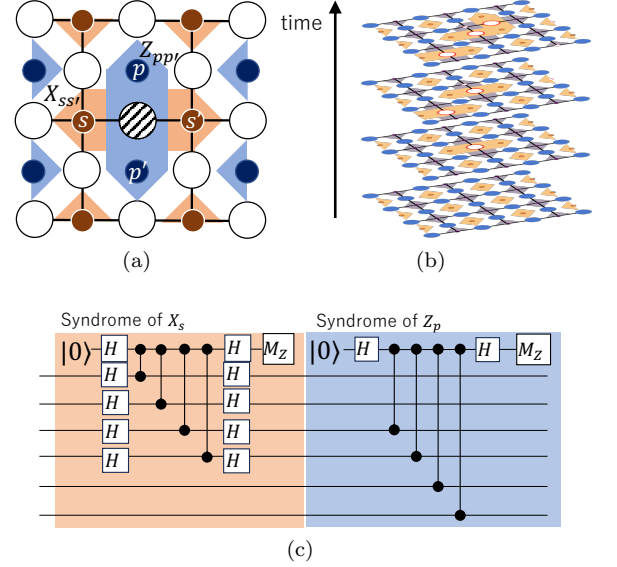


FIG. 2. (a) A figure of stabilizer generators $\tilde{\mathcal{G}}$ of the surface code. The large white circles are data qubits, respectively. The orange (blue) grey squares are stabilizer generators of $XXXX$ ($ZZZZ$) for star (plaquette) operators, respectively. The small orange (blue) grey circles are ancilla qubits for syndrome measurements. If a data qubit at the position of the circle with a diagonal line disappears, the stabilizer generators around it are merged and a super star (plaquette) operator of a large orange (blue) polygon is added as a new stabilizer generator to maintain the function as an error correction code. (b) The figure shows an example of the time evolution of a qubit array encoded by the surface code with code distance = 5. The blue circles are data qubits, and the small orange and blue circles are ancilla qubits for syndrome measurements of $X^{\otimes 4}$ and $Z^{\otimes 4}$, respectively. The bottom layer shows the situation before the syndrome measurement, and there are no erased qubits. The hierarchy represents the number of syndrome measurements, and the number of erased qubits (red circles) increases as the number of measurements increases. (c) A circuit of syndrome measurements for the surface code. The shaded parts in blue and orange are syndrome measurements of $X^{\otimes 4}$ and $Z^{\otimes 4}$, respectively.

vertices to edges each of which corresponds to a temporal measurement error of each syndrome. By estimating the most likely pairs for the vertices where the syndrome measurement outcomes flip, +1 to -1 or -1 to +1 on the Nest, both computation errors and measurement errors are detected and corrected. There are algorithms to estimate the most likely pair for the vertices [16–18]. A typical algorithm is the Minimum Weight Perfect Matching (MWPM) [19].

C. Previous works for erasure errors

Erasure errors can be classified into three: static erasure errors, dynamic erasure errors which can be cor-

rected immediately, and dynamic erasure errors which cannot be corrected immediately.

1. *Static erasure errors*

In a system where erasure errors happen statically, you can know the position of erasure errors before executing quantum computation and the number of erasure errors, and they are not changed during the execution. The typical case of static erasure errors is the fabrication error of such as superconducting quantum circuits [8, 20]. Static erasure errors are not errors occurring during computation but imperfections occurring before the computation. However, the static erasure error has many points in common with erasure errors: the absence of qubits causes them, their locations are heralded, and stabilizer modification is required to deal with them, as explained in the following sections. This type of erasure can be corrected by super stabilizers. There are two ways to construct super stabilizers, Stace and Barrett method [7] and Nagayama method [8]. The idea of Stace and Barrett's method is simple and easy to construct super stabilizers. The super stabilizers can be made by multiplying stabilizers related to erased data qubits like Fig. 2a. The star and plaquette stabilizers are merged into a super stabilizer in the same way, which means the deployment of it is symmetric. This method generates junk qubits as side effects, which are created on the extra degree of freedom caused by reducing two stabilizers for an erased data qubit. The super stabilizers decrease the threshold of state error rate even though junk qubits do not cause logical errors. On the other hand, Nagayama's method, in which super stabilizers and weight-reduced stabilizers are used together, is an improved version of Stace and Barrett's method. This method does not generate junk qubits, but the deployment of super stabilizers is asymmetric.

2. *Instantly correctable erasure error*

Some systems may have erasure errors happening dynamically during computation. In this case, the number of erasure errors changes during the computation. Mechanisms to detect the positions of erased qubits have been investigated, depending on the physical and architectural systems [3, 4, 21]. There are two types of erasure errors, i.e., in some systems, erasure errors remain, and in others, they don't.

A typical example of the first type is neutral atom quantum computers; erasure errors remain unless special operations are executed to fix erasure errors. Such a special operation is, i.e., to refill the erased position with a new atom instantly. Such refilling is achieved by conveying atoms with optical tweezers. In the erasure conversion approach [4, 22], the qubit information is exactly erased, but the atom may remain in its position. In

that case, it works to get erased qubits, which are in a completely mixed state, incorporated with the surrounding stabilizers, and projected to the proper code word state of the quantum error correcting code. However, conveying atoms with optical tweezers in this approach may disturb qubits along the path across the atom arrays.

A typical example of the latter type is one-way quantum computation with a 3-D cluster state [21, 23]. Because all qubits are going to be measured and disrupted anyway, erasure errors in a layer corresponding to a Big-T do not remain in the next Big-T. Thus, this model has the erasure-tolerance of up to 25 % erasure rate [23], though we don't actually "correct" the erased qubits.

3. *Accumulating, dynamic erasure errors*

Some systems, typically neutral atom array quantum computers, cannot correct dynamic erasure and leakage errors sequentially after detecting their events since conveying atoms into the online array disturbs other qubits. Consequently, the number of erasure errors in the arrays increases over time. In such cases, the surface code doesn't work properly because the distribution of erased qubits always changes over time, and error detection and decoding don't work properly around erased qubits.

In this study, we propose a scheme of surface code to deal with dynamic erasure errors and leakage errors that cannot be corrected in ordinary error correction cycles. This model corresponds to the Rydberg atomic quantum computer with optical tweezer arrays, which cannot convey atoms to the online array on which logical qubits are encoded.

IV. ERROR CORRECTION UNDER ACCUMULATED DYNAMIC ERASURE ERRORS

A. *The main problem*

Let us consider the situation where the erasure errors occur dynamically and cannot be corrected sequentially after detecting erasures. This situation corresponds to the Rydberg atomic quantum computer with optical tweezer arrays, which cannot convey atoms to the online array on which logical qubits are encoded because it may cause adverse effects such as decoherence or repulsion between atoms.

B. *Generating stabilizer generators*

In the case of the erasure errors occurring on the data qubits, you can maintain the function of the error correction by removing stabilizer generators related to the erased data qubits from the stabilizer group $\mathcal{S} = \langle \mathcal{G} \rangle$ and adding the super star (plaquette) operators to the

stabilizer group by multiplying the removed stabilizer generators. Here, we use Stace's method to compose stabilizers into a super stabilizer. Let us assume that a data qubit has been erased, as in the center of Fig. 2a. Two star stabilizer generators act on this erased data qubit, let's call them $X_i, X_j \in \mathcal{G}$. To exclude the erased data qubit from the code, we remove X_i and X_j from \mathcal{G} and add

$$X_{ij} = X_i X_j \quad (3)$$

to \mathcal{G} . On the plaquette stabilizer side as well, two stabilizers share the erased data qubit. Thus, you can compose these in the same way. Even when multiple erasures exist, instead of the stabilizers that share the erased data qubits, we can insert the stabilizer created by multiplying them to generate the deformed stabilizer group. We denote the new generators formed in this way as $\tilde{\mathcal{G}}$. The stabilizer group $\tilde{\mathcal{S}} = \langle \tilde{\mathcal{G}} \rangle$, which have $\tilde{\mathcal{G}}$ as their generators, newly stabilize the planar code state of the qubit array containing erasures.

C. Composition of super stabilizer and decoding on dynamic erasure

Dynamic erasure errors may occur while executing the stabilizer circuits. Therefore, we should perform erasure detection before measuring syndromes for all stabilizer generators, i.e., just before each syndrome measurement in each Big-T. Based on the distribution of detected erased qubits, we can construct the super stabilizer as described above and then perform syndrome measurements corresponding to the stabilizer generators that include the super stabilizer. Let us consider updating the stabilizer generators for each Big-T to adapt to erasure errors dynamically occurring. We have to detect erasure errors and their distribution on the array in every Big-T to compose the stabilizer generators based on the result of detecting the erasure distribution. The procedure to compose the stabilizer generator is described in Chap. IV B. In this study, to efficiently find the stabilizer pair to be composed, we compose them using the Union Find algorithm, as described in the pseudo-code in Algorithm. 1.

For a surface code with a code distance of d , we repeat syndrome measurements and erasure detections d times as described in Chap. III B, and based on these results, we create a Nest \mathcal{N} . If an erasure error occurs to a data qubit, we can create a Nest \mathcal{N} adapting to the super stabilizer $\tilde{\mathcal{S}}$ by setting the weight of the corresponding edge to 0 [7, 23]. In our error model, erasures accumulate, unlike the model in [23]. Thus, once an erasure error occurs, the weight of the edge is kept to be 0 after that. By matching vertices where the eigenvalues in syndrome measurement flip with a Minimum Weight Perfect Matching (MWPM) problem solver in \mathcal{N} , we can estimate where the Pauli errors happen.

V. NUMERICAL SIMULATION AND ITS ANALYSIS

A. Error models and assumptions in our simulation

In our simulation, we performed a circuit-based Monte Carlo error simulation to investigate the behavior of logical error and catastrophic corruption of the array. We considered Pauli errors, which occur in the qubit space, and erasure errors for errors occurring in physical qubits. We assumed that the Pauli errors occurring in the qubit space are depolarizing errors. The depolarizing error on a single-qubit is defined as an error channel where the three Pauli operators X, Y, Z are applied with equal probability $p_{\text{dep}}/3$, i.e.,

$$\mathcal{E}(\rho) = (1 - p_{\text{dep}})\rho + \frac{p_{\text{dep}}}{3} \sum_{M \in X, Y, Z} M \rho M^\dagger. \quad (4)$$

Similarly, the depolarizing error that acts on two-qubits with probability p_{dep} is defined as,

$$\mathcal{E}(\rho) = (1 - p_{\text{dep}})\rho + \frac{p_{\text{dep}}}{15} \sum_{M \in \mathcal{P}} M \rho M^\dagger \quad (5)$$

Here, the set \mathcal{P} is,

$$\mathcal{P} = \{IX, IY, IZ, XI, XX, XY, XZ, YI, YX, YY, YZ, ZI, ZX, ZY, ZZ\} \quad (6)$$

As described above, the erasure and heralded leakage errors can be considered an erasure error channel as Equation (1). In this simulation, we assumed that both erasure and leakage errors can be detected simultaneously before performing the syndrome measurement for all ancilla qubits and that the leakage error can be converted to an erasure error. Erasure errors occur with probability p_e for each gate operation, and once an erasure occurs, it cannot be recovered immediately. This model corresponds to the situation involving difficulties in refilling single atoms to the atomic tweezer array, such as additional erasure caused by the tweezer transportation [9].

B. Composition of super stabilizers

We determine the stabilizer generators to be composed based on the results of the detected erased qubits. We compose the stabilizer generators using Stace's method. We find the set of stabilizer generators to be composed with a Union Find structure, as shown in the pseudo-code in Algorithm 1. We can execute this algorithm to generate stabilizer generators for a system with erasure in $O(\log N)$ time steps for N qubits.

Algorithm 1 The method to compose super stabilizers via Union Find algorithm

```

1: function UNION_FIND(stabilizers)
2:    $uf \leftarrow \text{UnionFindStructure}(\text{stabilizers})$ 
3:   for all stabilizer0  $\leftarrow$  stabilizers do
4:      $\text{data\_qubits} \leftarrow \text{stabilizer.data\_qubits}$ 
5:     for all qubit  $\leftarrow$   $\text{data\_qubits}$  do
6:       if qubit is erased then
7:         stabilizer1  $\leftarrow$  Find_another_stabilizer(qubit)
8:          $uf.\text{union}(\text{stabilizer0}, \text{stabilizer1})$ 
9:       end if
10:    end for
11:  end for
12:  return uf
13: end function
14: function CREATE_STABILIZERS(ideal_stabilizers)
15:    $uf \leftarrow \text{UNION\_FIND}(\text{ideal\_stabilizers})$ 
16:    $\text{roots} \leftarrow uf.\text{roots}()$ 
17:   new_stabilizers  $\leftarrow$  MERGE_STABILIZERS(root, ideal_stabilizers)
18:   return new_stabilizers
19: end function

```

This function merges stabilizers belonging to the same tree using Stace's way.

The composition of the stabilizer generators reduces the effective code distance. The length of the shortest logical operator (composed of corresponding physical operator chain; hence, we can discuss the “length” of logical operators here) that transverses the larger stabilizer generator to be composed of normal ones is shorter than the shortest logical operator on the usual surface code with no erasures. The existence of a shorter logical operator means that the effective code distance becomes shorter. If the erasure errors happen continuously between the boundaries such as Fig. 3, a larger stabilizer generator that connects between boundaries will be composed. This lattice no longer has enough code distance and does not have a logical qubit to tolerate Pauli errors, i.e., the effective code distance becomes 2. Therefore, if erasure errors exist across the array, we grant that the logical qubit has been destroyed in this study.

Ancilla qubits are also exposed to erasure errors. However, its effect is possibly mitigated by reusing ones for other stabilizers because ancilla qubits can be shared by multiple stabilizers because they are initialized every time they are used. Thus, we check whether any ancilla held by the super (or normal) stabilizer is alive, and if it is not, we try to find a sharable ancilla qubit placed within the second nearest neighbor of the original ancilla qubit. If any sharable ancilla qubit is not found, we regard this logical qubit as also destroyed.

C. Decoding Pauli errors

The nest \mathcal{N} gets a more irregular shape in every Big-T by composing some stabilizer generators to super stabilizers as described above. To adopt this deformation,

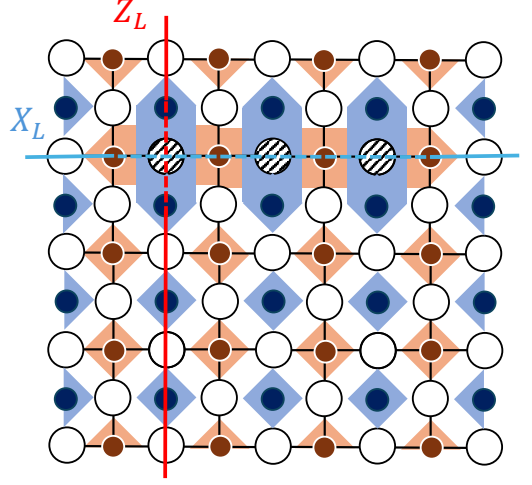


FIG. 3. A surface code of code distance $d = 5$ with erasure errors, which include shortened logical operators by super stabilizers. The blue and red line represents the shortest X and Z logical operators, X_L and Z_L . The X_L are shortened to $d = 3$ and the Z_L are shortened to $d = 2$ because of super stabilizers to adapt to erasure errors. The Z_L of $d = 2$ no longer has the tolerance against Z errors.

vertices in \mathcal{N} get removed or merged. Actually, by setting the weight of the edge corresponding to erased data qubits on the nest \mathcal{N} to 0, matching and decoding of $\tilde{\mathcal{N}}$ including the super stabilizers is still possible [7]. For a surface code with a code distance of d , we perform erasure detections and syndrome measurements d times. Erasure detection is theoretically possible with the circuit in Fig. 1. In this study, we did not employ this circuit explicitly and assumed that erasure detection always succeeds immediately without executing dedicated erasure-detecting circuits in the simulation. After erasure detections and syndrome measurements, we created a Nest $\tilde{\mathcal{N}}$ as described above, in which vertices hold the flips of measurement results. We used the Minimum Weight Perfect Matching (MWPM) Decoder to decode error syndromes in the Nest into error placements in our simulation [19].

We first check if a logical qubit was destroyed due to erasure errors and then whether a logical Pauli X error occurred. We can acquire the complete error distribution by tracking the Pauli frames, which are exactly the error information, classically in simulation, in contrast to real devices. The occurrence of the logical X error is determined by the parity of the number of X error chains crossing the logical Z operator on a boundary. The information of error syndromes involves perfect syndrome measurements at the last Big-T, not to misunderstand correctable, computational errors as measurement errors.

D. Numerical results

First, we calculated the threshold between the logical qubit error rate and the physical Pauli error rate, for each erasure error rate. The result of sweeping p_{dep} with fixed p_e is shown in Fig. 4. The results show that qubits cannot tolerate the increase in erasure error rate, depending on the number of repetitions of Big-T which depends on the code distance if the erasure error rate is too high. This model has just a pseudo-threshold, which is the threshold-like behavior around the crossing point-like region, even if the model, in principle, does not obey the threshold theorem in the asymptotic limit. Each data point in the graph is calculated from the number of error events n_{logical} in 10^5 attempts, each of which executes the whole circuit, i.e., $p_{\text{logical}} = n_{\text{logical}}/10^5$. Note that the numerical results are not smooth in the region of small p_{dep} . This is because the logical error probabilities in this region were too low to acquire enough error events in numerical simulation to make the graph smooth.

It is known that this error model does not have a threshold for erasures ($p_{e,\text{th}} = 0$) analytically. The ratio of qubits disappearing after repeating Big-T d times, which applies α gates to a qubit, is

$$R = 1 - (1 - p_e)^{\alpha d}. \quad (7)$$

Therefore, in the limit of $d \rightarrow \infty$, $R \rightarrow 1$. This means that erasure errors cannot be attenuated, regardless of how much the code distance is extended, as long as erasure errors continue to accumulate.

We also calculated the evolution of the logical error rate when decoding and error correction operations are repeated. The Fig. 5 shows the evolution of the logical error rate against the number of error correction (Big-T) loops when the depolarizing error rate per each gate operation is fixed at $p_{\text{dep}} = 1 \times 10^{-4}$ and the erasure error rate per each gate operation p_e is shifted from 0 to 1.0×10^{-5} . It can be seen that the logical error rate increases with the accumulation of erased physical qubits in the array, particularly as error detection and correction operations are repeatedly performed. Also, the Fig. 5 shows that there are many occurrences of the logical qubit destruction due to array destruction or the absence of alternative ancilla qubits when the erasure error rate is high or when the code distance is extended. This is because the longer the code distance, the deeper the circuit is to correct measurement errors, increasing the ratio of erased qubits on the array. Meanwhile, the figure shows that the logical error rate is suppressed by extending the code distance in some parameter regions such as $p_e < 1 \times 10^{-5}$ and the number of error correction iterations is lower than 10.

VI. k -SHIFT ERASURE RECOVERY

Our numerical simulation demonstrated that the repetition of the stabilizer circuit accumulates erased qubits,

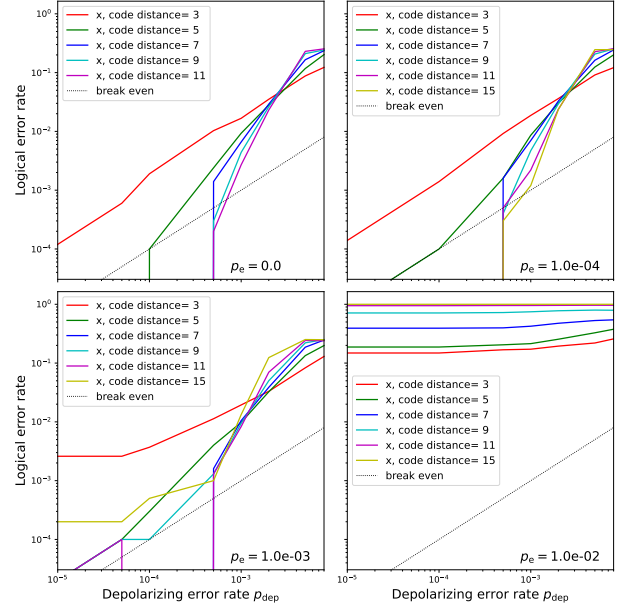


FIG. 4. The numerical result of Pauli error rate threshold for each erasure error rate p_e . Each colored line represents the logical error rate p_{logical} vs. the depolarizing error rate per gate operation p_{dep} (horizontal axis) with code distances 3, 5, 7, 9, 11 and 15. The erasure error rate p_e is fixed in each graph. The black dash line represents the break even, $p_{\text{logical}} = p_{\text{dep}}$.

the effective code distance decreases continuously, and finally, the code loses the Pauli error tolerance required. To solve this problem, we propose moving the logical qubit from the atom array with accumulated erasure errors to a new atom array free from erased qubits by combining the expansion and reduction operations of the surface code by code deformation [15] as shown in Fig. 6, namely, k -shift erasure recovery. Our proposal is a series of two steps below:

1. Repeat the surface code procedure tolerable against state errors, leakage errors, and erasure errors and execute quantum computation, with adapting accumulating erasure errors.
2. Transfer the logical qubit to another perfect atom array when the amount of erasure errors likely makes the error tolerance of the surface code below the required level of error tolerance. Then, refresh the old atom array that contains erased qubits to make the atomic qubit array perfect again.

This series of steps divides the functionality to execute quantum computation with protection against state errors and endure against erasure errors, and the functionality to correct erasure errors. Our scheme makes the logical qubit not suffer from the unexpected effects caused by fixing the atom array by evacuating the logical qubit from the imperfect array.

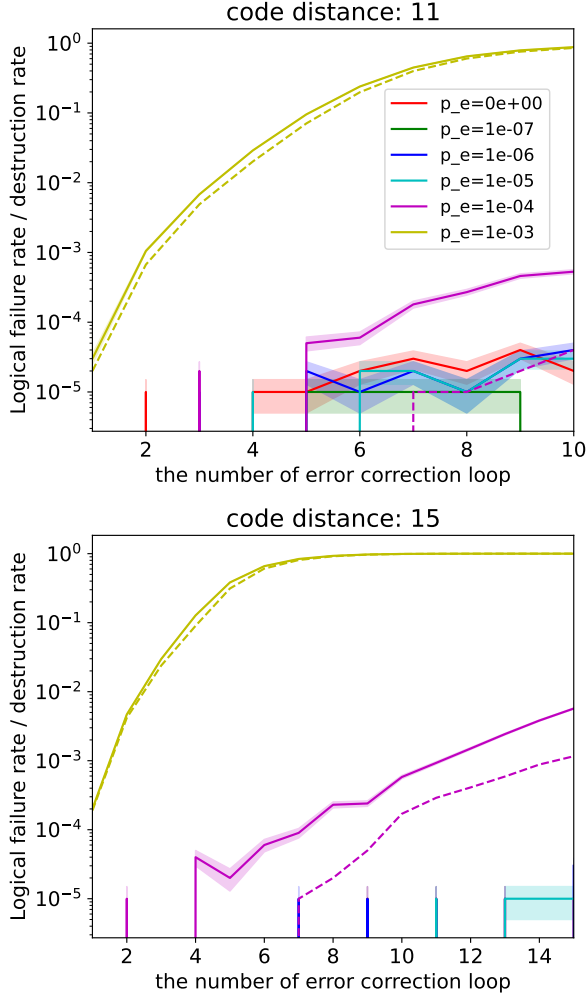


FIG. 5. The numerical result between the number of repetitions of the syndrome measurement and the logical failure rate (solid line) which includes both the logical Pauli error and the logical qubit destruction (dashed line) after the repetition. The upper and lower figures show the result with the code distance $d = 11$ and $d = 15$, respectively. The depolarizing error rate per gate operation is fixed at $p_e = 1 \times 10^{-4}$ in both graphs. Each colored line represents the erasure error rate p_e . The band with each line represents the standard deviation of the logical error rate. Each dashed line represents the logical qubit destruction rate described in Sec. V B.

Consider a qubit array \mathcal{A}_1 on which a logical qubit of the planar surface code is encoded, and another qubit array \mathcal{A}_2 on which nothing is encoded exist at first. We must iterate its syndrome measurement and error correction to correct Pauli errors on \mathcal{A}_1 . However, this iteration increases the erasure ratio and finally makes its logical error rate higher than the requirement, such as 10^{-15} [24]. Our protocol performs code deformation to move the logical qubit on \mathcal{A}_1 to the new perfect array \mathcal{A}_2 before the logical error probability of the logical qubits becomes higher than the required error rate, due to the

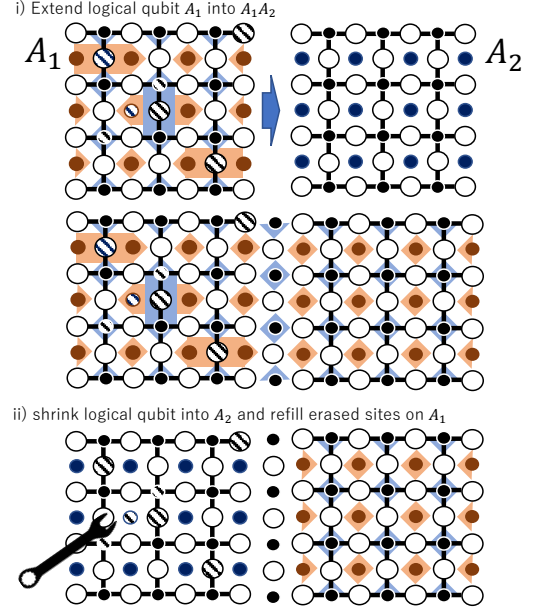


FIG. 6. The process of transferring a logical qubit via code deformation.

accumulation of erased qubits. First, initialize qubits in \mathcal{A}_2 appropriately to $|0\rangle$ or $|+\rangle$. Then, perform d syndrome measurements and decode and correct errors based on the measurement results to complete expansion of the logical qubits of the size $d \times d$ on \mathcal{A}_1 into logical qubits of $d \times 2d$ crossing on \mathcal{A}_1 and \mathcal{A}_2 . After that, measure the data qubit on \mathcal{A}_1 in Z or X basis depending on the direction of the boundary expanding, to complete shrinking the logical qubit to the size $d \times d$ on \mathcal{A}_2 . From the result of direct measurement on data qubits, determine and record the parity of the X or Z logical operator.

Now, qubits in \mathcal{A}_1 do not hold logical information. So, we can execute any operation to the qubits, even destructive operations, without any concerns. Thus, the imperfect array with erased qubits in \mathcal{A}_1 can be recovered by rearranging or refilling the array with a single atom from the atom reserver. For neutral atom array quantum computers, optical tweezers have been demonstrated to work well for such precise movement and insertion of atoms [25]. Our scheme separates the places to maintain the coherence of the logical qubits via syndrome measurements and the places for physical operations possibly destructive to quantum data to repair the array, such as rearrangement and refilling the array with atoms via tweezers. This provides us with the capability of taking more aggressive rearrangement strategies than the method of sequentially replenishing erased qubits.

In the same way, the erased qubit on the new array \mathcal{A}_2 will increase after repeating the error correction. Again, we can make the system resistant to erasure errors by transferring the logical qubit to another array before the logical error probability becomes too high due to the same reason above. The explanation above uses just two

pieces of qubit array and corresponds to 2-shift erasure recovery. This procedure can be expanded to k -shift erasure recovery with k pieces of qubit array, depending on the time needed to fix erasures on the array and the time until the array can no longer tolerate the accumulation of erasure errors and Pauli errors. We name this scheme " k -shift erasure recovery."

VII. DISCUSSION AND CONCLUSION

In this paper, we have numerically verified the error correction of surface codes on systems where erasure errors continuously occur, such as neutral atom quantum computers using optical tweezer arrays. Our work revealed that the threshold for erasure probability is theoretically 0 because the accumulation of erasure errors cannot be stopped and because erased qubits cannot be corrected unless they are offline arrays. In addition, it is also revealed that the logical error probability can be suppressed by increasing the code distance and repeating error correction if the erasure error rate is sufficiently low. However, iterating the syndrome detection and correction operations increases the number of erased qubits even if on such parameter regions. To solve the problem that error correction becomes impossible due to the accumulation of erased qubits, we proposed the k -shift erasure recovery scheme to protect the logical qubit from erasure by transferring the logical qubit to a perfect array using code deformation.

Our scheme allows us to rearrange physical qubits without concern about their decoherence caused by the transportation of physical qubits, which occurs as a side effect of the transport of atoms. Our scheme separates the rearrangement of qubits, which is too noisy for surrounding qubits, from the coherence-preserving operation of logical qubits including state error correction and logical operations. This separation allows for a more daring rearrangement strategy than conventional methods, such as sequentially replenishing erased qubits.

In the following, we discuss what we have not considered in this study and the open problems. The numerical calculations were performed assuming that each operation's probability of erasure errors is uniform. However, it is known that the Rydberg atomic quantum computer is prone to leakage errors and erasure of qubits when performing 2-qubit gates [4]. Therefore, it is a future work to investigate the effect of bias on the erasure error probability.

We decoded error syndromes using the MWPM de-

coder. Actually, various improved decoders, such as the Union-Find decoder [17], have also been proposed. The Union-Find decoder is an almost-linear time decoder for correcting Pauli errors and erasure errors. Research into utilizing such decoders instead of MWPM is valuable for achieving erasure tolerance in Rydberg atomic quantum computers [4]. It would be interesting to compare their performance for accumulating, dynamical erasure errors.

It is also necessary to investigate the efficient scheduling and allocating of ancilla qubits for syndrome collection under this scheme. Rydberg gates allow syndrome collection with more efficient circulation of ancilla qubits and more efficient scheduling of syndrome measurements than the recent study that assumes only nearest-neighbor interactions [8].

We exemplify our proposal with code deformation to transfer logical qubits from an imperfect array due to erasure errors to a new perfect array. It would be interesting to compare our scheme of code deformation with that of other methods, such as ones with quantum teleportation or transversal swap gates since Clifford gates can be performed transversely on the surface codes. These methods may transfer logical qubits more efficiently than the code deformation we equipped in our numerical simulation.

We utilized modularity to repair quantum computers and to ensure the sustainability of quantum information processing. Our scheme can be applied to other faults as well as erasure correction, leveraging quantum networks and distributed quantum computing; like classical cloud computing moves or relocates services and data from one computer to another to sustain services permanently. Our scheme enables the preservation of logical qubits from critical faults by transferring them from a faulted quantum device to a fresh one. Such distributed maintainability will be fundamental technology for the reliable and continuous usage of fault-tolerant quantum computers.

ACKNOWLEDGMENTS

The authors thank Thomas M. Stace, Takashi Yamamoto, Rikizo Ikuta, and Toshiki Kobayashi for their helpful advice. This research was supported by JST Moonshot R&D (JPMJMS2066, JPMJMS226C). FK was supported by JST, the establishment of university fellowships towards the creation of science technology innovation, Grant Number JPMJFS2125. FK and SN acknowledge the members of Quantum Internet Task Force for comprehensive discussions of quantum networks.

-
- [1] D. Bluvstein, H. Levine, G. Semeghini, T. T. Wang, S. Ebadi, M. Kalinowski, A. Keesling, N. Maskara, H. Pichler, M. Greiner, V. Vuletić, and M. D. Lukin, *Nature* **604**, 451 (2022).
 - [2] D. Bluvstein, S. J. Evered, A. A. Geim, S. H. Li,

- H. Zhou, T. Manovitz, S. Ebadi, M. Cain, M. Kalinowski, D. Hangleiter, J. P. B. Ataides, N. Maskara, I. Cong, X. Gao, P. S. Rodriguez, T. Karolyshyn, G. Semeghini, M. J. Gullans, M. Greiner, V. Vuletić, and M. D. Lukin, *Nature* (2023).

- [3] I. Cong, H. Levine, A. Keesling, D. Bluvstein, S.-T. Wang, and M. D. Lukin, *Physical Review X* **12**, 021049 (2022).
- [4] Y. Wu, S. Kolkowitz, S. Puri, and J. D. Thompson, *Nat. Commun.* **13**, 4657 (2022).
- [5] S. Ma, G. Liu, P. Peng, B. Zhang, S. Jandura, J. Claes, A. P. Burgers, G. Pupillo, S. Puri, and J. D. Thompson, *Nature* **622**, 279 (2023).
- [6] P. Scholl, A. L. Shaw, R. B.-S. Tsai, R. Finkelstein, J. Choi, and M. Endres, *Nature* **622**, 273 (2023).
- [7] T. M. Stace and S. D. Barrett, *Phys. Rev. A* **81**, 022317 (2010).
- [8] S. Nagayama, A. G. Fowler, D. Horsman, S. J. Devitt, and R. Van Meter, *New J. Phys.* **19**, 023050 (2017).
- [9] D. Barredo, S. de Léséleuc, V. Lienhard, T. Lahaye, and A. Browaeys, *Science* **354**, 1021 (2016), <https://www.science.org/doi/pdf/10.1126/science.aah3778>.
- [10] D. Jaksch, J. I. Cirac, P. Zoller, S. L. Rolston, R. Cote, and M. D. Lukin, *Phys. Rev. Lett.* **85**, 2208 (2000).
- [11] M. Saffman, *J. Phys. B At. Mol. Opt. Phys.* **49**, 202001 (2016).
- [12] D. Barredo, V. Lienhard, S. de Léséleuc, T. Lahaye, and A. Browaeys, *Nature* **561**, 79 (2018).
- [13] M. Grassl, T. Beth, and T. Pellizzari, (1996), [arXiv:quant-ph/9610042](https://arxiv.org/abs/quant-ph/9610042) [quant-ph].
- [14] E. Dennis, A. Kitaev, A. Landahl, and J. Preskill, (2001), [arXiv:quant-ph/0110143](https://arxiv.org/abs/quant-ph/0110143) [quant-ph].
- [15] C. Horsman, A. G. Fowler, S. Devitt, and R. Van Meter, (2011), [arXiv:1111.4022](https://arxiv.org/abs/1111.4022) [quant-ph].
- [16] A. G. Fowler, A. C. Whiteside, A. L. McInnes, and A. Rabbani, *Physical Review X* **2**, 041003 (2012).
- [17] N. Delfosse and G. Zémor, (2017), [arXiv:1703.01517](https://arxiv.org/abs/1703.01517) [quant-ph].
- [18] A. D. iOlius, P. Fuentes, R. Orús, P. M. Crespo, and J. E. Martinez, (2023), [arXiv:2307.14989](https://arxiv.org/abs/2307.14989) [quant-ph].
- [19] V. Kolmogorov, *Math. Program. Comput.* **1**, 43 (2009).
- [20] J. M. Auger, H. Anwar, M. Gimeno-Segovia, T. M. Stace, and D. E. Browne, *Physical Review A* **96**, 042316 (2017).
- [21] A. C. Whiteside and A. G. Fowler, (2014), [arXiv:1409.4880](https://arxiv.org/abs/1409.4880) [quant-ph].
- [22] K. Sahay, J. Jin, J. Claes, J. D. Thompson, and S. Puri, (2023), [arXiv:2302.03063](https://arxiv.org/abs/2302.03063) [quant-ph].
- [23] S. D. Barrett and T. M. Stace, *Phys. Rev. Lett.* **105**, 200502 (2010).
- [24] A. G. Fowler, M. Mariantoni, J. M. Martinis, and A. N. Cleland, *Phys. Rev. A* **86** (2012).
- [25] D. Barredo, S. de Léséleuc, V. Lienhard, T. Lahaye, and A. Browaeys, *Science* **354**, 1021 (2016).